

Probing Hidden Topology with Quantum Detectors

Dyuman Bhattacharya,^{1,*} Jorma Louko,^{2,†} and Robert B. Mann^{1,3,4,‡}

¹*Department of Physics and Astronomy, University of Waterloo, Waterloo, Ontario, N2L 3G1, Canada*

²*School of Mathematical Sciences, University of Nottingham, Nottingham NG7 2RD, United Kingdom*

³*Institute for Quantum Computing, University of Waterloo, Waterloo, Ontario, N2L 3G1, Canada*

⁴*Perimeter Institute for Theoretical Physics, Waterloo, Ontario, N2L 2Y5, Canada*

(Dated: October 2024)

We consider the transition rate of a static Unruh-DeWitt detector in two $(2+1)$ -dimensional black hole spacetimes that are isometric to the static Bañados-Teitelboim-Zanelli black hole outside the horizon but have no asymptotically locally anti-de Sitter exterior behind the horizon. The spacetimes are the \mathbb{RP}^2 geon, with spatial topology $\mathbb{RP}^2 \setminus \{\text{point at infinity}\}$, and the Swedish geon of Åminneborg *et al*, with spatial topology $T^2 \setminus \{\text{point at infinity}\}$. For a conformal scalar field, prepared in the Hartle-Hawking-type state that is induced from the global vacuum on the anti-de Sitter covering space, we show numerically that the detector's transition rate distinguishes the two spacetimes, particularly at late exterior times, and we trace this phenomenon to the differences in the isometries that are broken by the quotient construction from the universal covering space. Our results provide an example in which information about the interior topology of a black hole is accessible to a quantum observer outside the black hole.

I. INTRODUCTION

Black holes are amongst the most fascinating objects in nature, in large part because they cloak certain regions of space and time from all distant observers. While black holes created in a gravitational collapse are not time symmetric, their eternal counterparts contain both a future horizon and past horizon, and continuing the spacetime analytically past these horizons reveals new structure, a prime example of which is the second asymptotically flat region in the Kruskal(-Szekeres-Fronsdal) [1–3] extension of positive mass Schwarzschild spacetime. The structure past the horizon has a pivotal role in recognising Hawking temperature as the distinguished temperature for quantum fields in thermal equilibrium with the black hole [4], and it provides the cornerstone to the view of black hole entropy as a fundamentally quantum-gravitational concept [5].

What lies beyond the black hole horizon is, by definition, inaccessible to classical observers outside the horizon. However, in an eternal black hole spacetime, with both a future horizon and a past horizon, states of quantum fields that are regular on the extended spacetime are constrained by the spacetime structure behind the horizons. For such states, it is therefore possible for a local quantum observer to distinguish what lies behind the horizon by probing the state of a quantum field outside the horizon [6–11]. In this paper we address this phenomenon for a class of black hole spacetimes known as topological geons [12], in which there is no second asymptotic region behind the horizon [10, 13, 14].

The geon black hole spacetimes that we consider are $(2+1)$ -dimensional eternal black holes, which are solu-

tions to Einstein's equations with a negative cosmological constant, and have an exterior region that is isometric to that of the spinless non-extremal Bañados-Teitelboim-Zanelli (BTZ) black hole [15, 16]. We consider two families, both obtained as a quotient of an open set in $(2+1)$ -dimensional anti-de Sitter spacetime (AdS_3) by a discrete group of isometries. One family is the \mathbb{RP}^2 geon [7], which is a \mathbb{Z}_2 quotient of the BTZ black hole and has spatial topology $\mathbb{RP}^2 \setminus \{\text{point at infinity}\}$. The other is the “Swedish geon” of Åminneborg *et al* [17], which has spatial topology $T^2 \setminus \{\text{point at infinity}\}$. In both of these spacetimes, the exterior Killing vector that generates exterior BTZ time translations does not extend to a Killing vector on the full spacetime. The state that a quantum field inherits from the global vacuum on AdS_3 is hence not static in the exterior region [7, 8], in contrast to the Hartle-Hawking-type state inherited by the BTZ spacetime [18, 19], and this nonstaticity bears an imprint of the spacetime structure behind the horizon. We shall analyse how a local quantum observer outside the horizon can access this imprint.

We consider a massless conformal scalar field. We model a local quantum observer by an Unruh-DeWitt (UDW) detector [20, 21], a pointlike two-level system that is linearly coupled to the field, and we work to linear order in the coupling. We compute the detector's transition rate on a trajectory that is static in the exterior geometry: the time dependence in this transition rate is then precisely due to the geon-like spacetime structure behind the horizon.

For both the \mathbb{RP}^2 geon and the Swedish geon, our numerical results show that the transition rate in the asymptotic past reduces to that on the BTZ hole. Assuming the detector to be switched on in the asymptotic past, the late time behaviour, however, differs for the two spacetimes. The late time transition rate in the Swedish geon asymptotes to that in the BTZ hole. The late time transition rate in the \mathbb{RP}^2 geon, by contrast, asymptotes

* d7bhatta@uwaterloo.ca

† jorma.louko@nottingham.ac.uk

‡ rbmann@uwaterloo.ca

to a different constant for a gapless detector, and it displays persisting oscillations for a detector with a nonvanishing gap; the latter property is consistent with what was previously found for the \mathbb{RP}^2 geon [11], and with what happens for uniformly accelerated detectors in flat spacetimes with a similar structure behind the Rindler horizon [22, 23]. This difference between the late time transition rates is a dramatic demonstration of how the detector in the exterior can distinguish different spacetime topologies behind the horizon.

As a side product, we give explicit formulas for the isometries by which the Swedish geon is quotiented from AdS_3 , in a representation in which the exterior region takes a standard form, and we display a fundamental domain for the spacelike hypersurface of time symmetry. This representation of the isometries can be employed to investigate other properties of the quantum state that the Swedish geon inherits from the global vacuum on AdS_3 , such as the stress-energy tensor.

Our paper is organized as follows. Section II gives a brief review of an UDW detector coupled to a scalar field, writing down the transition rate of a detector that is switched on and off sharply. Section III presents the static BTZ black hole, the \mathbb{RP}^2 geon and the Swedish geon as quotients of subsets of AdS_3 , deferring technicalities to three appendices. Section IV gives the image sum constructions for the static detector's transition rate on these spacetimes, for a conformal scalar field in the state induced from the global vacuum on AdS_3 . Numerical results for the detector's transition rate are presented in Section V. Section VI gives the conclusions and a brief discussion.

II. UNRUH-DEWITT DETECTOR

We probe the quantum field by an Unruh-DeWitt (UDW) detector, which is a point-like quantum system that has two states: a state $|0\rangle_D$ with energy 0, and a state $|1\rangle_D$ with energy Ω , where Ω is a real-valued parameter. For $\Omega > 0$, $|0\rangle_D$ is the ground state and $|1\rangle_D$ is the excited state; for $\Omega < 0$, the roles of $|0\rangle_D$ and $|1\rangle_D$ are reversed.

The detector follows a spacetime trajectory $x_D(\tau)$, which we parametrize by its proper time τ , and it is coupled to a real scalar field $\phi(x)$ through the interaction Hamiltonian

$$H_I(\tau) = \lambda \chi(\tau) \mu(\tau) \otimes \phi[x_D(\tau)], \quad (1)$$

where λ is a coupling constant, $\chi(\tau)$ is a switching function that determines how the interaction is turned on and off, and $\mu(\tau)$ is the detector's monopole moment operator, given by

$$\mu(\tau) = e^{i\Omega\tau} \sigma^+ + e^{-i\Omega\tau} \sigma^-, \quad (2)$$

where $\sigma^+ = |1\rangle_D \langle 0|_D$ and $\sigma^- = |0\rangle_D \langle 1|_D$ are the respective raising and lowering ladder operators. The detector's Hilbert space is \mathbb{C}^2 .

Before the interaction is turned on, we prepare the detector in the state $|0\rangle_D$ and the field ϕ in the state that we denote here by $|0\rangle$ and specify individually in the applications in the later sections. Working in first-order perturbation theory, the probability to find the detector in the state $|1\rangle_D$ after the interaction has ceased, regardless the final state of the field, is [24, 25]

$$P(\Omega) = \lambda^2 \mathcal{F}(\Omega), \quad (3)$$

where the response function $\mathcal{F}(\Omega)$ is given by

$$\mathcal{F}(\Omega) = \int d\tau d\tau' \chi(\tau) \chi(\tau') e^{-i\Omega(\tau-\tau')} W(\tau, \tau'), \quad (4)$$

and $W(\tau, \tau') = \langle 0| \phi(x_D(\tau)) \phi(x_D(\tau')) |0\rangle$ is the pullback of the field's Wightman function to the detector's worldline.

We take χ to be the characteristic function of an interval of time, as the response function remains well defined in this limit in $2+1$ spacetime dimensions despite the discontinuities at the switch-on and switch-off moments. We further consider not the response function itself but its derivative with respect to the switch-off moment, denoted by $\dot{\mathcal{F}}$, which has an interpretation as (a multiple of) the detector's transition rate, operationally measurable using ensembles of detectors [23, 25, 26]. For a detector switched on at time τ_0 and off at time τ , the transition rate is given by [27]

$$\dot{\mathcal{F}}(\Omega) = \frac{1}{4} + 2 \int_0^{\Delta\tau} ds \text{Re} [e^{-i\Omega s} W(\tau, \tau - s)], \quad (5)$$

where $\Delta\tau = \tau - \tau_0$. If the detector is switched on in the asymptotic past, $\tau_0 \rightarrow -\infty$, the transition rate (5) becomes

$$\dot{\mathcal{F}}(\Omega) = \frac{1}{4} + 2 \int_0^\infty ds \text{Re} [e^{-i\Omega s} W(\tau, \tau - s)]. \quad (6)$$

Note that while $W(\tau, \tau')$ has a distributional singularity at $\tau = \tau'$, the integrals in (5) and (6) do not have distributional contributions from $s = 0$. This is because the singularity in $W(\tau, \tau')$ is that of

$$\frac{-i}{4\pi(\tau - \tau' - i\epsilon)} \xrightarrow{\epsilon \rightarrow 0^+} \frac{-i}{4\pi} P\left(\frac{1}{\tau - \tau'}\right) + \frac{1}{4} \delta(\tau - \tau'), \quad (7)$$

where P stands for the Cauchy principal value: the term $\frac{1}{4}$ in (5) and (6) has come from the Dirac delta in (7), and the integrals in (5) and (6) are nonsingular at $s = 0$ on taking the real part.

III. QUOTIENTS OF AdS_3

In this section we describe three black hole spacetimes that are quotients of an open subset in AdS_3 .

A. AdS₃

Recall that AdS₃ may be defined as the hyperboloid

$$X_1^2 + X_2^2 - T_1^2 - T_2^2 = -\ell^2 \quad (8)$$

in $\mathbb{R}^{2,2}$ with the metric

$$ds^2 = dX_1^2 + dX_2^2 - dT_1^2 - dT_2^2, \quad (9)$$

where ℓ is a positive constant of dimension length. This spacetime is a solution to Einstein's equations with the cosmological constant $\Lambda = -\ell^2$ [19].

It is useful to introduce two local coordinate systems on open subsets of AdS₃ as follows.

First, in the subset \mathbf{B}_1 , defined as $T_1 > |X_1|$, we introduce the coordinates (U, V, ϕ) by

$$\begin{aligned} T_1 &= \ell \left(\frac{1 - UV}{1 + UV} \right) \cosh(\sqrt{M} \phi), \\ X_1 &= \ell \left(\frac{1 - UV}{1 + UV} \right) \sinh(\sqrt{M} \phi), \\ T_2 &= \ell \left(\frac{V + U}{1 + UV} \right), \\ X_2 &= \ell \left(\frac{V - U}{1 + UV} \right), \end{aligned} \quad (10)$$

where $-1 < UV < 1$, $-\infty < \phi < \infty$, and M is a positive parameter. The metric takes the form

$$ds^2 = -\frac{4\ell^2}{(1 + UV)^2} dU dV + r_h^2 \left(\frac{1 - UV}{1 + UV} \right)^2 d\phi^2. \quad (11)$$

Second, in the subset of \mathbf{B}_1 where $U < 0$ and $V > 0$, we introduce the coordinates (t, r, ϕ) , where

$$\begin{aligned} \frac{r}{r_h} &= \frac{1 - UV}{1 + UV}, \\ \frac{r_h t}{\ell^2} &= \frac{1}{2} \ln \left(-\frac{V}{U} \right), \end{aligned} \quad (12)$$

where $r_h = \ell\sqrt{M}$, so that $r_h < r < \infty$ and $-\infty < \phi < \infty$. In terms of the embedding space coordinates, this means

$$\begin{aligned} X_1 &= \ell \frac{r}{r_h} \sinh \left(\frac{r_h}{\ell} \phi \right), \\ X_2 &= \ell \sqrt{\frac{r^2}{r_h^2} - 1} \cosh \left(\frac{r_h}{\ell^2} t \right), \\ T_1 &= \ell \frac{r}{r_h} \cosh \left(\frac{r_h}{\ell} \phi \right), \\ T_2 &= \ell \sqrt{\frac{r^2}{r_h^2} - 1} \sinh \left(\frac{r_h}{\ell^2} t \right), \end{aligned} \quad (13)$$

and the metric reads

$$ds^2 = -\left(\frac{r^2 - r_h^2}{l^2} \right) dt^2 + \left(\frac{r^2 - r_h^2}{l^2} \right)^{-1} dr^2 + r^2 d\phi^2. \quad (14)$$

We refer to (14) as the AdS-Rindler metric [28].

B. BTZ black hole

The spinless BTZ spacetime is obtained from \mathbf{B}_1 with the metric (11) by the identification $(U, V, \phi) \sim (U, V, \phi + 2\pi)$. This spacetime is an eternal black-and-white-hole spacetime, with a bifurcate Killing horizon at $|U| = |V|$, and (U, V, ϕ) are Kruskal-type coordinates [15, 16, 19]. The mass of the black hole is M .

We may write the spacetime as the quotient space

$$\mathcal{M}_{\text{BTZ}} = \mathbf{B}_1 / \mathbb{Z}, \quad (15)$$

where $\mathbb{Z} \simeq \{\Gamma^n : n \in \mathbb{Z}\}$ with

$$\Gamma : (U, V, \phi) \mapsto (U, V, \phi + 2\pi). \quad (16)$$

The quadrant where $U < 0$ and $V > 0$, covered by the coordinates (t, r, ϕ) with the identification $(t, r, \phi) \sim (t, r, \phi + 2\pi)$, is an exterior region. The metric is given by (14), and the horizon is at $r \rightarrow r_h$.

C. \mathbb{RP}^2 geon

The \mathbb{RP}^2 geon [7] is the quotient of the BTZ spacetime by the isometry group $\{e, J\} \simeq \mathbb{Z}_2$, where e is the identity and

$$J : (U, V, \phi) \mapsto (V, U, \phi + \pi). \quad (17)$$

We may write

$$\mathcal{M}_{\mathbb{RP}^2} = \mathcal{M}_{\text{BTZ}} / \mathbb{Z}_2. \quad (18)$$

This spacetime is an eternal black and white hole spacetime with just a single exterior region, in which the metric is as in (14). While the exterior is static, with the time-like Killing vector ∂_t , this Killing vector does not extend to all of the geon spacetime, and the geometry behind the horizons hence makes the $t = 0$ hypersurface a distinguished hypersurface of time symmetry [7, 11, 28].

D. Swedish geon

The Swedish geon [17] is a single-exterior black-and-white hole quotient of AdS₃, with the exterior metric given by the BTZ exterior (14), but with behind-the-horizon identifications that give the spacetime the spatial topology of a punctured torus, the puncture being at the AdS infinity, $r \rightarrow \infty$ in (14). We review the construction of this spacetime in the three appendices, showing that the spacetime is a quotient of a subset of AdS₃ by the free group generated by the $O(2, 2)$ matrices A and B given by

$$A = \begin{pmatrix} 1 & 0 & 0 & 0 \\ 0 & \frac{\cosh(6z) + 2\cosh(4z) + \cosh(2z)}{4\sinh^2(z)} & \frac{\sqrt{\cosh(2z)}\cosh(4z)}{\sinh^2(z)} & \sinh(4z) \\ 0 & -\frac{\sqrt{\cosh(2z)}}{\sinh^2(z)} & -\coth^2(z) & 0 \\ 0 & -\frac{\cosh(5z) + 3\cosh(3z) + 4\cosh(z)}{2\sinh(z)} & -4[\cosh(2z)]^{3/2}\coth(z) & -\cosh(4z) \end{pmatrix}, \quad (19a)$$

$$B = \begin{pmatrix} 1 & 0 & 0 & 0 \\ 0 & \frac{\cosh(4z) + \cosh(2z)}{2\sinh^2(z)} & \frac{[\cosh(2z)]^{3/2}}{\sinh^2(z)} & \frac{\cosh(3z) + \cosh(z)}{\sinh(z)} \\ 0 & -\frac{[\cosh(2z)]^{3/2}}{\sinh^2(z)} & -\coth^2(z) & -2\sqrt{\cosh(2z)}\coth(z) \\ 0 & \frac{\cosh(3z) + \cosh(z)}{\sinh(z)} & 2\sqrt{\cosh(2z)}\coth(z) & 2\cosh(2z) + 1 \end{pmatrix}, \quad (19b)$$

acting by matrix multiplication on the column vectors

$$\begin{pmatrix} T_2 \\ T_1 \\ X_2 \\ X_1 \end{pmatrix}, \quad (20)$$

where $z = \frac{1}{4}\pi\sqrt{M}$. (We have dropped in (19) the underlines by which these matrices are denoted in (A14) in Appendix A.) The exterior region is again covered by the coordinates (t, r, ϕ) (13), so that M is the black hole mass. The isometry $(t, r, \phi) \mapsto (t, r, \phi + 2\pi)$ is generated by the matrix $BAB^{-1}A^{-1}$.

IV. RESPONSE RATE COMPARISONS

In this section we present the image sum expressions for the detector's transition rate on the BTZ black hole, the \mathbb{RP}^2 geon and the Swedish geon.

A. Image sum in the state induced from the AdS₃ global vacuum

On each of the three quotients of AdS₃, we consider the state induced from the AdS₃ global vacuum. Denoting by G the discrete group by which the quotient is taken, the Wightman function is given by the method-of-images sum

$$W_{\text{AdS}_3/G}(x, x') = \sum_{g \in G} W_{\text{AdS}_3}(x, gx'), \quad (21)$$

where W_{AdS_3} is the Wightman function on AdS₃.

The global vacuum Wightman function for a massless conformally-coupled scalar field in AdS₃ takes the form [19, 28]

$$W_{\text{AdS}_3}(x, x') = \frac{1}{4\pi\sqrt{2}\ell} \left(\frac{1}{\sqrt{\sigma(x, x')}} - \frac{\zeta}{\sqrt{\sigma(x, x') + 2}} \right), \quad (22)$$

where $\sigma(x, x')$ is $1/(2\ell^2)$ times the square of the geodesic distance between the spacetime points x and x' in the embedding space $\mathbb{R}^{2,2}$,

$$\sigma(x, x') = \frac{1}{2\ell^2} \left[(X_1 - X'_1)^2 - (T_1 - T'_1)^2 + (X_2 - X'_2)^2 - (T_2 - T'_2)^2 \right], \quad (23)$$

and the parameter $\zeta \in \{-1, 0, 1\}$ specifies the boundary condition at the asymptotically AdS infinity. $\zeta = 1$ and $\zeta = -1$ are respectively the Dirichlet and Neumann boundary conditions, each of which determines a quantum theory with unitary evolution. $\zeta = 0$ is the transparent boundary condition, with no reflection from the infinity, and a less clear physical interpretation [29].

In all three spacetimes, we consider a UDW detector on the static exterior worldline that is given in the BTZ exterior coordinates (14) by

$$(t, r, \phi) = \left(\frac{\ell}{\sqrt{R^2 - r_h^2}}\tau, R, 0 \right), \quad (24)$$

where $R > r_h$ is the detector's radial coordinate and τ is the detector's proper time. Taking the detector to be switched on in the asymptotic past, the detector's transition rate may then be obtained by inserting the trajectory (24) in (6) with (21) and (22).

We consider the three spacetimes in turn.

B. BTZ

On the BTZ spacetime, we have

$$W_{\text{BTZ}}(x, x') = \sum_{n=-\infty}^{\infty} W_{\text{AdS}_3}(x, \Gamma^n x'), \quad (25)$$

where Γ is given in (16). In the exterior, in the coordinates (13), the action of Γ reads

$$\Gamma : (t, r, \phi) \mapsto (t, r, \phi + 2\pi). \quad (26)$$

It follows that [27]

$$\begin{aligned} \dot{\mathcal{F}}_{\text{BTZ}}(\Omega) &= \frac{e^{-\ell\beta\Omega/2}}{2\pi} \sum_{n=-\infty}^{\infty} \int_0^{\infty} dy \cos(y\ell\beta\Omega/2) \\ &\times \left(\frac{1}{\sqrt{K_n + \cosh^2 y}} - \frac{\zeta}{\sqrt{Q_n + \cosh^2 y}} \right), \end{aligned} \quad (27)$$

where

$$\begin{aligned} K_n &:= \frac{R^2}{R^2 - r_h^2} \sinh^2 \left(n\pi \frac{r_h}{\ell} \right), \\ Q_n &:= K_n + \frac{r_h^2}{R^2 - r_h^2}, \\ \beta &:= 2\pi \frac{\sqrt{R^2 - r_h^2}}{r_h}. \end{aligned} \quad (28)$$

Note that the transition rate has no dependence on the switch-off moment τ . This is because the isometry Γ (16) commutes with translations along the trajectory (24).

C. \mathbb{RP}^2 geon

On the \mathbb{RP}^2 geon, we have

$$W_{\mathbb{RP}^2}(x, x') = W_{\text{BTZ}}(x, x') + W_{\text{BTZ}}(x, Jx'), \quad (29)$$

where J is given in (17). It follows that

$$\dot{\mathcal{F}}_{\mathbb{RP}^2}(\Omega) = \dot{\mathcal{F}}_{\text{BTZ}}(\Omega) + \Delta\dot{\mathcal{F}}_{\mathbb{RP}^2}(\Omega, \tau), \quad (30)$$

where the additional contribution due to the geon identification may be written as [11]

$$\begin{aligned} \Delta\dot{\mathcal{F}}_{\mathbb{RP}^2}(\Omega, \tau) &= \frac{1}{2\pi} \sum_{n=-\infty}^{\infty} \int_0^{\infty} dy \cos(y\ell\beta\Omega/2) \\ &\times \left[\frac{1}{\sqrt{\bar{K}_n + \cosh^2 \left(y - \frac{\pi\tau}{\beta\ell} \right)}} \right. \\ &\left. - \frac{\zeta}{\sqrt{\bar{Q}_n + \cosh^2 \left(y - \frac{\pi\tau}{\beta\ell} \right)}} \right] \end{aligned} \quad (31)$$

where

$$\begin{aligned} \bar{K}_n &:= \frac{R^2}{R^2 - r_h^2} \sinh^2 \left[\left(n + \frac{1}{2} \right) \pi \frac{r_h}{\ell} \right], \\ \bar{Q}_n &:= K_n + \frac{r_h^2}{R^2 - r_h^2}. \end{aligned} \quad (32)$$

Note that the transition rate now depends on the switch-off moment τ . If the detector is switched off in the distant past, $\tau \rightarrow -\infty$, the geon correction term $\Delta\dot{\mathcal{F}}_{\mathbb{RP}^2}$ (31) is small, and the response is nearly identical to that in BTZ spacetime. However, $\Delta\dot{\mathcal{F}}_{\mathbb{RP}^2}$ becomes significant near $\tau = 0$, and it stays significant as $\tau \rightarrow \infty$. This is because the isometry J (17) does not commute with translations along the trajectory (24): among all constant t surfaces in the geon's exterior, the surface $t = 0$ is the only one that extends to a smooth geodesically complete surface in the geon spacetime [7].

D. Swedish geon

Since the matrices A and B (19) are a pair of free generators for the fundamental group of the Swedish geon, the Swedish geon Wightman function takes the form (21), where each g is a unique string in A and B and their inverses, such that A and A^{-1} may not appear next to each other and B and B^{-1} may not appear next to each other, but subject to no other conditions. For g with exactly $N \geq 1$ generators in the string, there are $4 \cdot 3^{N-1}$ terms in the sum, in addition to the pure AdS_3 term $W_{\text{AdS}_3}(x, x')$; for g with up to $K \geq 1$ generators in the string, there are

$$\sum_{N=1}^K 4 \cdot 3^{N-1} = 2(3^K - 1) \quad (33)$$

terms in addition to the pure AdS_3 term.

The detector's transition rate is now obtained from (6) with (24), (21) and (22).

In numerical evaluation, we group the terms in the sum by the number of generators in the string, and we truncate the sum at a finite number K of generators, monitoring the accuracy of the truncation by increasing K . As terms with a large number of generators are suppressed by successive factors that are negative exponentials in \sqrt{M} , accurate evaluation requires fewer terms for larger values of M .

V. RESULTS

Figure 1 shows numerical results for the detector's transition rate as a function of the switch-off moment on AdS_3 , the BTZ black hole, the \mathbb{RP}^2 geon, and the Swedish geon. The detector is switched on in the asymptotic past and the detector's gap is set to zero. We have set $M = 7$, so that $r_h = \sqrt{7}\ell$, and the detector is placed

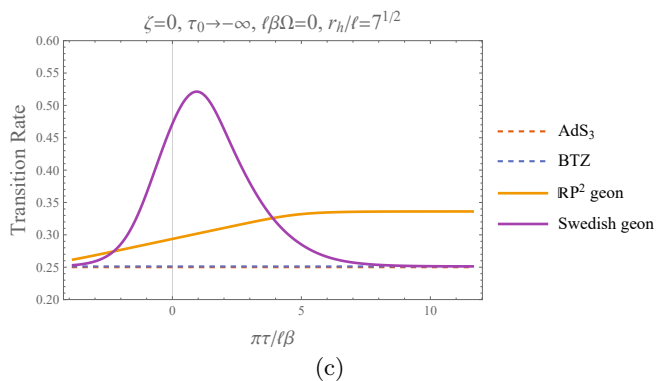
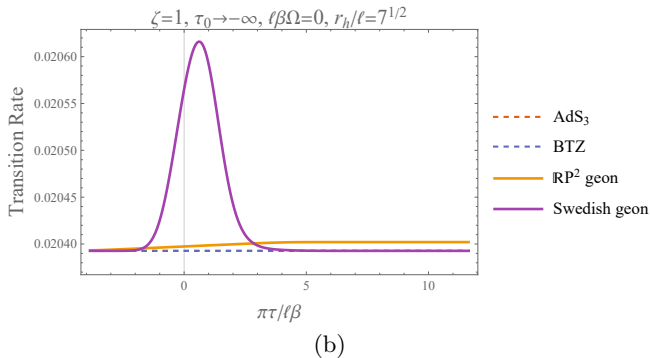
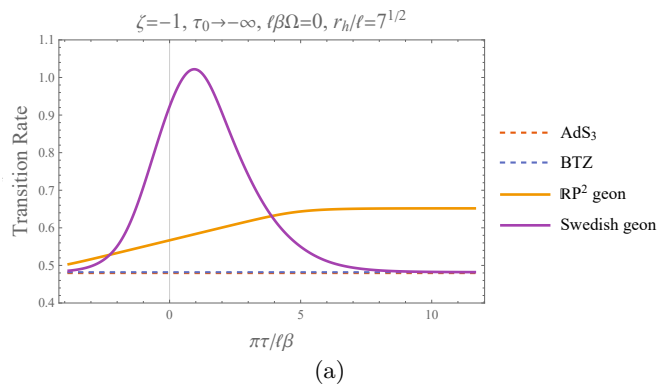


FIG. 1. The transition rate of a gapless detector, switched on in the asymptotic past, as a function of the switch-off moment, for AdS₃, the BTZ black hole, the \mathbb{RP}^2 geon, and the Swedish geon. The parameters are $r_h/\ell = \sqrt{7}$ and $R^2/r_h^2 = \frac{25}{7}$. Panels (a), (b) and (c) are for the Neumann ($\zeta = -1$), Dirichlet ($\zeta = 1$), and transparent ($\zeta = 0$) boundary condition, respectively. The transition rates on AdS₃ and the BTZ black hole so close that they are indistinguishable by the naked eye.

at $R = \frac{5}{\sqrt{7}}r_h$. The three panels show the boundary condition at infinity being respectively Neumann, Dirichlet, and transparent.

On AdS₃ and on the BTZ hole, the transition rate is independent of the switch-off moment, by the time translation symmetry of the global vacuum on AdS, and by the corresponding time translation symmetry inherited by the Hartle-Hawking state on the BTZ black hole.

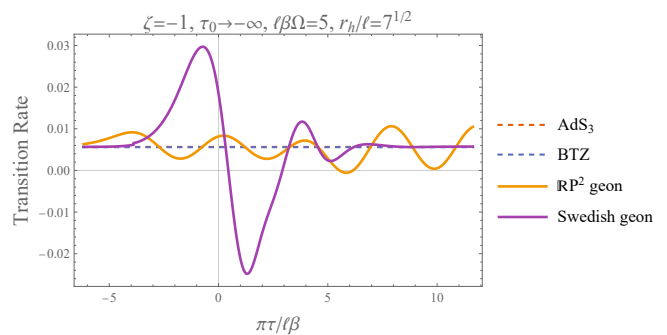


FIG. 2. As in Figure 1(a) but with $\ell\beta\Omega = 5$, giving the excitation rate of a detector with a nonzero gap. The transition rates on AdS₃ and the BTZ black hole are again so close that they are indistinguishable by the naked eye.

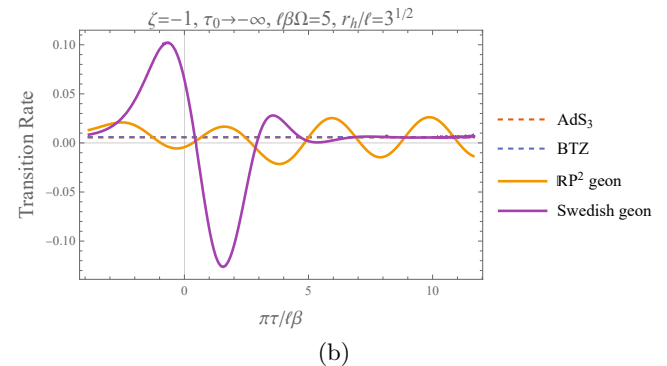
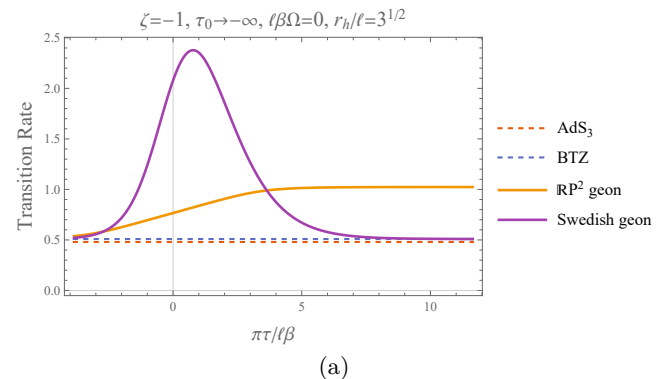


FIG. 3. As in Figures 1(a) (Panel (a)) and 2 (Panel (b)) but with a smaller black hole, $r_h/\ell = \sqrt{3}$, with detector position still such that $R^2/r_h^2 = \frac{25}{7}$.

This independence is clear in all three panels in Figure 1. With the parameters chosen, the transition rates on AdS₃ and the BTZ hole are so close that they are indistinguishable by the naked eye. On the \mathbb{RP}^2 geon, the transition rate in the asymptotic past agrees with that for the BTZ black hole, but in the asymptotic future it differs: this phenomenon was previously noticed in [11], and traced to the fact that the Hartle-Hawking-type state on the \mathbb{RP}^2 geon exterior is not invariant under the exterior Killing time translations, and to the way in which the late time

additional contributions arise from the detector having operated in the distant past. Related observations in flat spacetimes with similar isometries were made in [22, 23].

Now, for the Swedish geon, Figure 1 shows that the transition rate agrees with that for the BTZ black hole both in the asymptotic past and in the asymptotic future, but it displays a distinct bump at intermediate times. The behaviour seen in the asymptotic past is as expected, stemming from the lack of exterior time translation symmetry of the Hartle-Hawking type state induced from the global vacuum. The behaviour seen in the asymptotic future is numerical evidence that the Swedish geon correlations between the asymptotic future and asymptotic past are significantly more involved than those on the \mathbb{RP}^2 geon. An analytic explanation of this phenomenon and the underlying correlations would require a deeper geometric study of the discrete group action by which the Swedish geon is quotiented from AdS_3 .

For a detector with a nonzero gap, a plot for $\ell\beta\Omega = 5$ and the Neumann boundary condition is shown in Figure 2. The graph shows that the transition rate on the \mathbb{RP}^2 geon and the Swedish geon display more oscillations as a function of the switch-off moment. For the \mathbb{RP}^2 geon these oscillations continue to asymptotically late times, as noted in [11], but on the Swedish geon we see the late time transition rate again asymptotically approaches the stationary BTZ value.

Figure 3 is as in Figures 1(a) and 2 but with a smaller black hole. The qualitative features are similar, but the bumps in the Swedish geon transition rate are now noticeably larger. The AdS_3 transition rate and the BTZ black hole transition rate are now distinguishable by eye in Figure 3.

Regarding numerical accuracy, the more massive Swedish geon plots include contributions from image terms with up to $K = 5$ generators in the strings that define the group elements. We checked that the results did not change visibly on taking $K = 6$. We also made additional spot checks at late times with $K = 8$, involving a total of 13,120 image terms. While we found this to be sufficient for the more massive black hole mass $M = 7$ used in the plots, numerical accuracy for smaller values of M would require more image terms. The less massive ($M = 3$) Swedish geon plots include contributions from image terms with up to $K = 8$ generators, for sufficient accuracy.

VI. CONCLUSIONS AND DISCUSSION

We have considered the transition rate of a static UDW detector in two $(2+1)$ -dimensional black hole spacetimes that are isometric to the static BTZ black hole outside the horizon but have the spatial topology of a topological geon, with no second exterior region behind the black-and-white-hole horizons. The detector was coupled linearly to a conformal scalar field, prepared in the Hartle-Hawking-type state that is induced from the global vac-

uum on AdS_3 , with Dirichlet, Neumann or transparent boundary conditions at the infinity. The detector was treated in first-order perturbation theory and assumed switched on in the asymptotic past.

The spacetimes were the \mathbb{RP}^2 geon [7] and the Swedish geon of Åminneborg *et al* [17], each obtained as a quotient of an open subset in AdS_3 under a discrete isometry group. For both of these topological geon spacetimes, we found that the detector's response differs from that for the BTZ black hole, and the responses for the two spacetimes differ from each other. In particular, the detector's late time transition rate in the \mathbb{RP}^2 geon differs from that in the BTZ black hole, as previously found in [11], and the geometric reasons for this were identified in a related context in [22, 23]; by contrast, our numerical results show that the late time response in the Swedish geon approaches that on the BTZ black hole. An analytic explanation of this late time phenomenon would require a deeper geometric study of the discrete group action by which the Swedish geon is quotiented from AdS_3 .

Our numerical results also show that, for the Swedish geon, at intermediate times the transition rate is much larger than for the \mathbb{RP}^2 geon with the same mass. This is perhaps not unexpected, as the image sum for the field's Wightman function on the \mathbb{RP}^2 geon consists of a strict subset of the terms in the image sum on the Swedish geon, but a more quantitative explanation would again require a deeper study of the discrete group action by which the Swedish geon is constructed from AdS_3 .

The salient lesson from our results is that specific information about the interior topology of a black hole is accessible to an observer outside the black hole by allowing them to probe a quantum state that has been prepared with knowledge of the global topology of the spacetime.

A limitation of our results is the restriction to static observers. The response rate of infalling detectors for the spinless [30] and spinning [31] BTZ black holes has been recently investigated, as well as for the \mathbb{RP}^2 geon [32]. These results suggest that the Swedish geon case will exhibit more detailed differences as compared to its \mathbb{RP}^2 geon counterpart. This remains an interesting subject for future work.

ACKNOWLEDGMENTS

We thank Fredrik Strömberg for discussions on fundamental domains. This work was supported in part by the Natural Sciences and Engineering Research Council of Canada. The work of JL was supported by United Kingdom Research and Innovation Science and Technology Facilities Council [grant numbers ST/S002227/1, ST/T006900/1 and ST/Y004523/1]. For the purpose of open access, the authors have applied a CC BY public copyright licence to any Author Accepted Manuscript version arising.

Appendix A: Swedish geon generators

In this appendix we construct a convenient pair of free generators of the isometry group by which the Swedish geon is quotiented from AdS_3 . We first consider the spacelike hypersurface on which the geometry is locally that of the Poincaré disk, and we then extend the generators to the spacetime.

1. Fundamental domain on the Poincaré disk

Recall that the Poincaré metric on the open unit disk $|z| < 1$ of \mathbb{C} is

$$ds^2 = \frac{4|dz|^2}{(1 - |z|^2)^2}. \quad (\text{A1})$$

The metric has constant negative curvature, with Ricci scalar -2 . The metric is invariant under the fractional linear $SU(1, 1)$ action

$$z \mapsto U(z) = \frac{\alpha z + \bar{\beta}}{\beta z + \bar{\alpha}}, \quad (\text{A2})$$

where $U \in SU(1, 1)$ is written as

$$U = \begin{pmatrix} \alpha & \bar{\beta} \\ \beta & \bar{\alpha} \end{pmatrix}, \quad (\text{A3})$$

where α and β are complex numbers with $|\alpha|^2 - |\beta|^2 = 1$. The only degeneracy in this action is that U and $-U$ give the same fractional linear transformation. The isometry group of the Poincaré disc is hence $PSU(1, 1)$, and elements in $PSU(1, 1)$ may be represented as in (A3) when understood modulo overall sign.

To establish notation, we define three one-parameter families of $SU(1, 1)$ matrices by

$$R(\theta) := \begin{pmatrix} e^{i\theta/2} & 0 \\ 0 & e^{-i\theta/2} \end{pmatrix}, \quad (\text{A4a})$$

$$D_H(\psi) := \begin{pmatrix} \cosh(\psi/2) & \sinh(\psi/2) \\ \sinh(\psi/2) & \cosh(\psi/2) \end{pmatrix}, \quad (\text{A4b})$$

$$D_V(\psi) := \begin{pmatrix} \cosh(\psi/2) & i \sinh(\psi/2) \\ -i \sinh(\psi/2) & \cosh(\psi/2) \end{pmatrix}. \quad (\text{A4c})$$

The action of $R(\theta)$ on the disk is a rotation about the origin, and θ is the rotation angle, measured positive counterclockwise. The action of $D_H(\psi)$ is a boost with fixed points at $z = \pm 1$, such that positive values of the rapidity ψ move points to the right, towards $z = 1$. The action of $D_V(\psi)$ is a boost with fixed points at $z = \pm i$, such that positive values of the rapidity ψ move points upwards, towards $z = i$. The subscripts H and V stand respectively for “horizontal” and “vertical.”

With this notation, let $a > 2 \operatorname{arsinh} 1$, and let

$$\tilde{A} := D_H(a), \quad (\text{A5a})$$

$$\tilde{B} := D_V(a). \quad (\text{A5b})$$

\tilde{A} and \tilde{B} act on the disk as illustrated in Figure 4(a), mapping the four symmetrically-chosen geodesic circle segments to each other as shown. The condition $a > 2 \operatorname{arsinh} 1$ is the condition for the circle segments not to intersect, neither on the open disk nor on its boundary. From the figure it is hence clear that the group generated by \tilde{A} and \tilde{B} acts on the disk freely and properly discontinuously, and the domain between the four circle segments in the figure serves as a fundamental domain for the group action. This is the construction given in [17].

The symmetric fundamental domain shown in Figure 4(a) intersects the boundary of the disk in four segments, but it is clear from the identifications that these four segments connect to form a circle, and the quotient space hence has a single trumpet-like infinity. A fundamental domain adapted to the infinity is displayed in Figure 4(b), where the identifications of the boundary segments are as shown, and the $SU(1, 1)$ matrices A and B are given by

$$A = R(q)D_H(-\chi_A)D_V(-a)D_H(\chi_A)R(-q), \quad (\text{A6a})$$

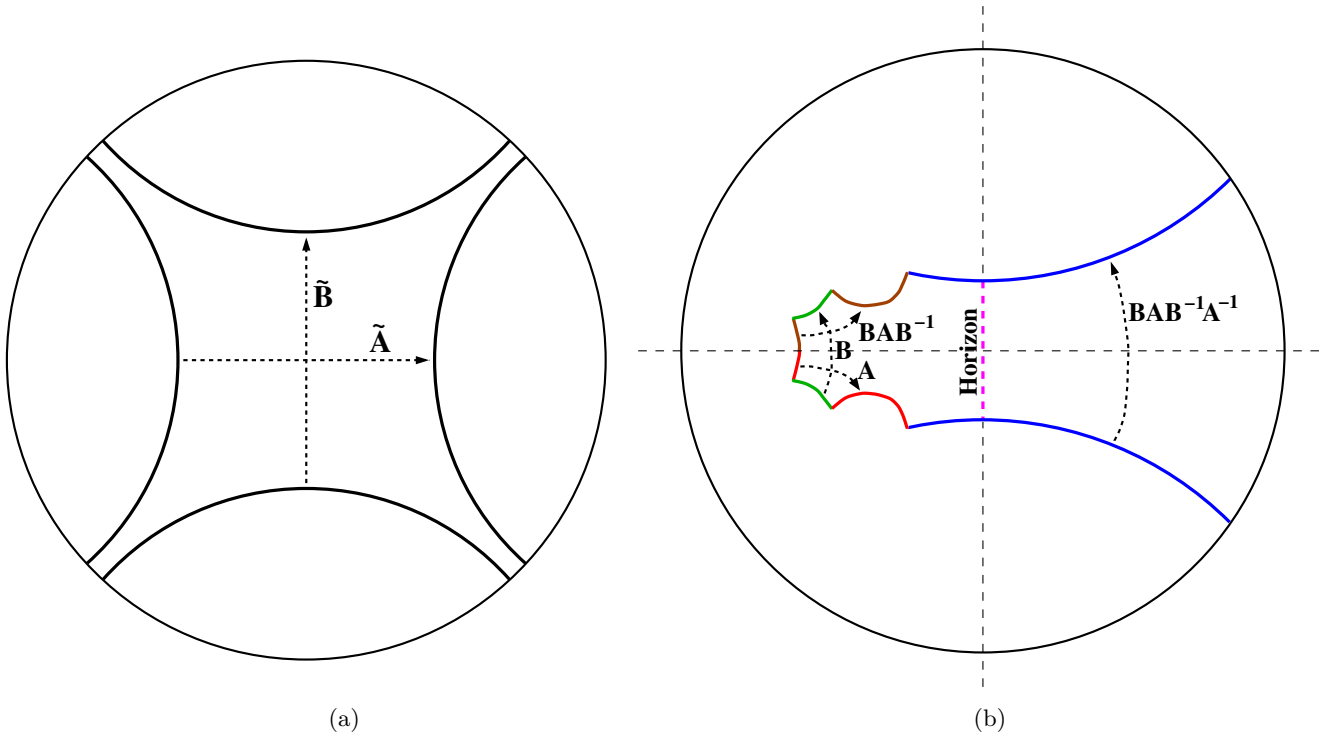


FIG. 4. Two fundamental domains on the Poincaré disk. **(a)** In panel (a), the fundamental domain is between the four symmetrically-arranged geodesic circle segments, and the identifications of the segments use the generators \tilde{A} and \tilde{B} (A5) as shown. The fundamental domain reaches the boundary of the disk in four segments, and the identifications join these segments into a circle. **(b)** In panel (b), the fundamental domain is between the seven geodesic circle segments, and the identifications of the segments use the generators A and B (A6) as shown. The fundamental domain is adapted to the infinity, where it reaches the boundary of the disk in a single segment, and the identification by $BAB^{-1}A^{-1} = -D_V(\psi_h)$, with ψ_h given by (A10), joins this segment into a circle. The horizon is on the axis of $D_V(\psi_h)$ as shown.

$$B = D_H(-\chi_B)D_V(a)D_H(\chi_B), \quad (\text{A6b})$$

with

$$q = \arctan\left(\frac{\sqrt{S^4 - 1}}{S}\right), \quad (\text{A7a})$$

$$\chi_A = \operatorname{artanh}\left(\frac{S^2}{\sqrt{S^4 + S^2 - 1}}\right), \quad (\text{A7b})$$

$$\chi_B = \operatorname{artanh}\left(\frac{1}{S}\right), \quad (\text{A7c})$$

where

$$S := \sinh(a/2), \quad C := \cosh(a/2). \quad (\text{A8})$$

The map between the two infinity-reaching boundary segments is by

$$BAB^{-1}A^{-1} = -D_V(\psi_h), \quad (\text{A9})$$

where

$$\psi_h = 4 \operatorname{arcosh}(S^2). \quad (\text{A10})$$

The transformations leading from Figure 4(a) with (A5) to Figure 4(b) with (A6) are given in Appendix B.

In Appendix C it is shown that the quotient surface is a punctured torus, and $A/\{\pm 1\}$ and $B/\{\pm 1\}$ are a pair of free generators of the fundamental group of this surface.

2. Generators in the spacetime

Recall that we realise AdS_3 as the hyperboloid (8) in $\mathbb{R}^{2,2}$ with the metric (9). We write the action of the $O(2,2)$ isometry group on AdS_3 in terms of the embedding space coordinates as

$$\begin{pmatrix} T_2 \\ T_1 \\ X_2 \\ X_1 \end{pmatrix} \mapsto \underline{U} \begin{pmatrix} T_2 \\ T_1 \\ X_2 \\ X_1 \end{pmatrix}, \quad (\text{A11})$$

where \underline{U} denotes $O(2,2)$ elements in the defining matrix representation.

In terms of this realisation, we embed the Poincaré disc of Figure 4(b) in AdS_3 by

$$T_2 = 0, \quad (\text{A12a})$$

$$\frac{T_1}{\ell} = \frac{1 + |z|^2}{1 - |z|^2}, \quad (\text{A12b})$$

$$\frac{X_2 + iX_1}{\ell} = \frac{2z}{1 - |z|^2}, \quad (\text{A12c})$$

as the spacelike hypersurface $T_2 = 0$ with $T_1 > 0$. The induced metric on this hypersurface is ℓ^2 times (A1). The isometries of the Poincaré disk by the $SU(1,1)$ matrices (A4) are induced from the AdS_3 isometries by the respective $O(2,2)$ matrices

$$\underline{R}(\theta) = \begin{pmatrix} 1 & 0 & 0 & 0 \\ 0 & 1 & 0 & 0 \\ 0 & 0 & \cos \theta & -\sin \theta \\ 0 & 0 & \sin \theta & \cos \theta \end{pmatrix}, \quad (\text{A13a})$$

$$\underline{D}_H(\psi) = \begin{pmatrix} 1 & 0 & 0 & 0 \\ 0 & \cosh \psi & \sinh \psi & 0 \\ 0 & \sinh \psi & \cosh \psi & 0 \\ 0 & 0 & 0 & 1 \end{pmatrix}, \quad (\text{A13b})$$

$$\underline{D}_V(\psi) = \begin{pmatrix} 1 & 0 & 0 & 0 \\ 0 & \cosh \psi & 0 & \sinh \psi \\ 0 & 0 & 1 & 0 \\ 0 & \sinh \psi & 0 & \cosh \psi \end{pmatrix}. \quad (\text{A13c})$$

It can then be verified that the Poincaré disc isometries by A and B (A6) are induced from the respective AdS_3 isometries by

$$\underline{A} = \begin{pmatrix} 1 & 0 & 0 & 0 \\ 0 & \frac{\cosh(6z) + 2 \cosh(4z) + \cosh(2z)}{4 \sinh^2(z)} & \frac{\sqrt{\cosh(2z)} \cosh(4z)}{\sinh^2(z)} & \sinh(4z) \\ 0 & -\frac{\sqrt{\cosh(2z)}}{\sinh^2(z)} & -\coth^2(z) & 0 \\ 0 & -\frac{\cosh(5z) + 3 \cosh(3z) + 4 \cosh(z)}{2 \sinh(z)} & -4[\cosh(2z)]^{3/2} \coth(z) & -\cosh(4z) \end{pmatrix}, \quad (\text{A14a})$$

$$\underline{B} = \begin{pmatrix} 1 & 0 & 0 & 0 \\ 0 & \frac{\cosh(4z) + \cosh(2z)}{2 \sinh^2(z)} & \frac{[\cosh(2z)]^{3/2}}{\sinh^2(z)} & \frac{\cosh(3z) + \cosh(z)}{\sinh(z)} \\ 0 & -\frac{[\cosh(2z)]^{3/2}}{\sinh^2(z)} & -\coth^2(z) & -2\sqrt{\cosh(2z)} \coth(z) \\ 0 & \frac{\cosh(3z) + \cosh(z)}{\sinh(z)} & 2\sqrt{\cosh(2z)} \coth(z) & 2 \cosh(2z) + 1 \end{pmatrix}, \quad (\text{A14b})$$

where $z = \frac{1}{8}\psi_h$. The Poincaré disc isometry by $BAB^{-1}A^{-1}$ (A9) is induced from the AdS₃ isometry by $D_V(\psi_h)$. It follows that the quotient of the Poincaré disc evolves into a single-exterior spinless BTZ black hole with $2\pi\sqrt{M} = \psi_h$, where M is the mass, and the exterior is covered by the BTZ coordinates (t, r, ϕ) in (13) and (14), with the identification $(t, r, \phi) \sim (t, r, \phi + 2\pi)$. In terms of M , (A14) then has $z = \frac{1}{4}\pi\sqrt{M}$.

Appendix B: Fundamental domain deformation

In this appendix we describe the deformation between the two fundamental domains shown in Figure 4.

We start from the Poincaré disc of Figure 4(a), with \tilde{A} and \tilde{B} given by (A5). We map the disc to the upper half-plane by the fractional linear transformation

$$w = V \times \frac{(1 - i(C + S))z + i - (C + S)}{(1 + i(C + S))z + i + (C + S)}, \quad (\text{B1})$$

where S and C are given by (A8), and $V := \sqrt{\frac{S+1}{S-1}}$. Writing $w = u + iv$, where $u \in \mathbb{R}$ and $v > 0$, the metric (A1) is mapped to the upper half-plane hyperbolic metric

$$ds^2 = \frac{du^2 + dv^2}{v^2}. \quad (\text{B2})$$

The fractional linear transformations by \tilde{A} and \tilde{B} are mapped respectively to fractional linear transformations by the $SL(2, \mathbb{R})$ matrices

$$\hat{A} = \begin{pmatrix} -C(S-1) & -S^2V \\ S^2V^{-1} & C(S+1) \end{pmatrix}, \quad (\text{B3a})$$

$$\hat{B} = \begin{pmatrix} C & SV \\ SV^{-1} & C \end{pmatrix}. \quad (\text{B3b})$$

The fixed points $z = \pm 1$ of \tilde{A} are mapped to the fixed points of \hat{A} , which are respectively at $w = -V(C-1)S^{-1}$ and $w = -V(C+1)S^{-1}$, and the fixed points $z = \pm i$ of \tilde{B} are mapped to the fixed points of \hat{B} , which are respectively at $w = \pm V$. The fundamental domain in Figure 4(a) is mapped to the fundamental domain D_1 in Figure 5, with the identifications described in the caption. Figures 5–7 then show how D_1 can be replaced by the new fundamental domain D_3 in Figure 7(b), as described in the captions. In particular, it follows that there is a horizon, generated by the boost

$$\hat{B}\hat{A}\hat{B}^{-1}\hat{A}^{-1} = - \begin{pmatrix} 2S^4 - 1 & 2CS^2\sqrt{S^2 - 1} \\ 2CS^2\sqrt{S^2 - 1} & 2S^4 - 1 \end{pmatrix}, \quad (\text{B4})$$

which has fixed points $w = \pm 1$ and the boost parameter ψ_h (A10).

Finally, we map D_3 in the upper half-plane back to the Poincaré disk by the fractional linear transformation

$$z = \frac{iw + 1}{-iw + 1}, \quad (\text{B5})$$

which maps $w = 0$ to $z = 1$, $w = i$ to $z = 0$ and $w = \infty$ to $z = -1$. This gives the fundamental domain in Figure 4(b). A and B are boosts with rapidity a , with fixed points respectively at

$$A : e^{iq} \frac{-S^2 \mp i\sqrt{S^2 - 1}}{\sqrt{S^4 + S^2 - 1}}, \quad (\text{B6a})$$

$$B : \frac{-1 \pm i\sqrt{S^2 - 1}}{S}, \quad (\text{B6b})$$

where q is given by (A7a). From this it follows that A and B have the expressions given in (A6)–(A8), using the fact that $D_H(\psi)$ maps the fixed points $\pm i$ of $D_V(\psi)$ to respectively $\tanh \psi \pm i/\cosh \psi$.

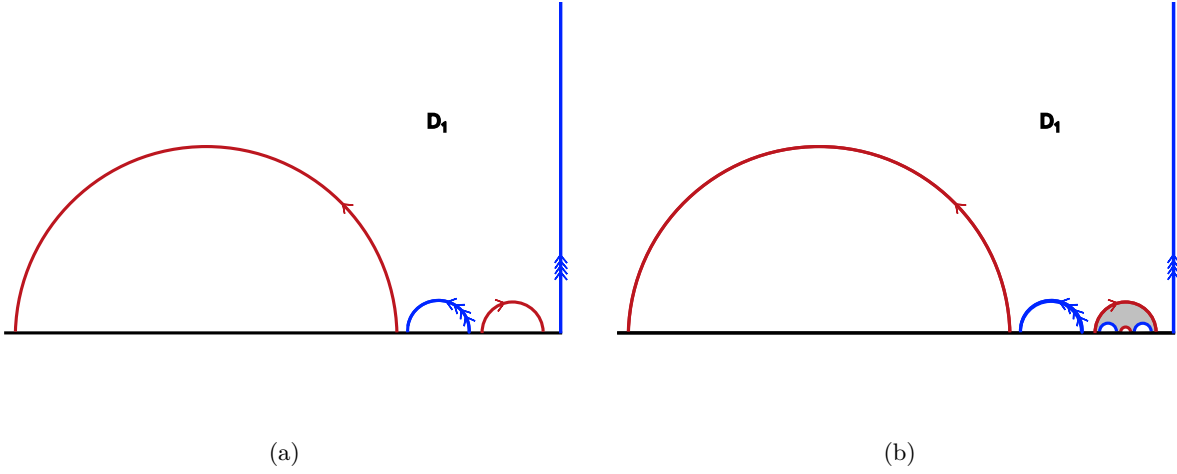


FIG. 5. **(a)** The upper half-plane fundamental domain D_1 to which the fundamental domain in Figure 4(a) is mapped by the fractional linear transformation (B1). \hat{A} maps the left single-arc to the right one, and \hat{B} maps the quadruple-arc to the positive imaginary axis. **(b)** D_1 together with its image under \hat{A} , shown shaded.

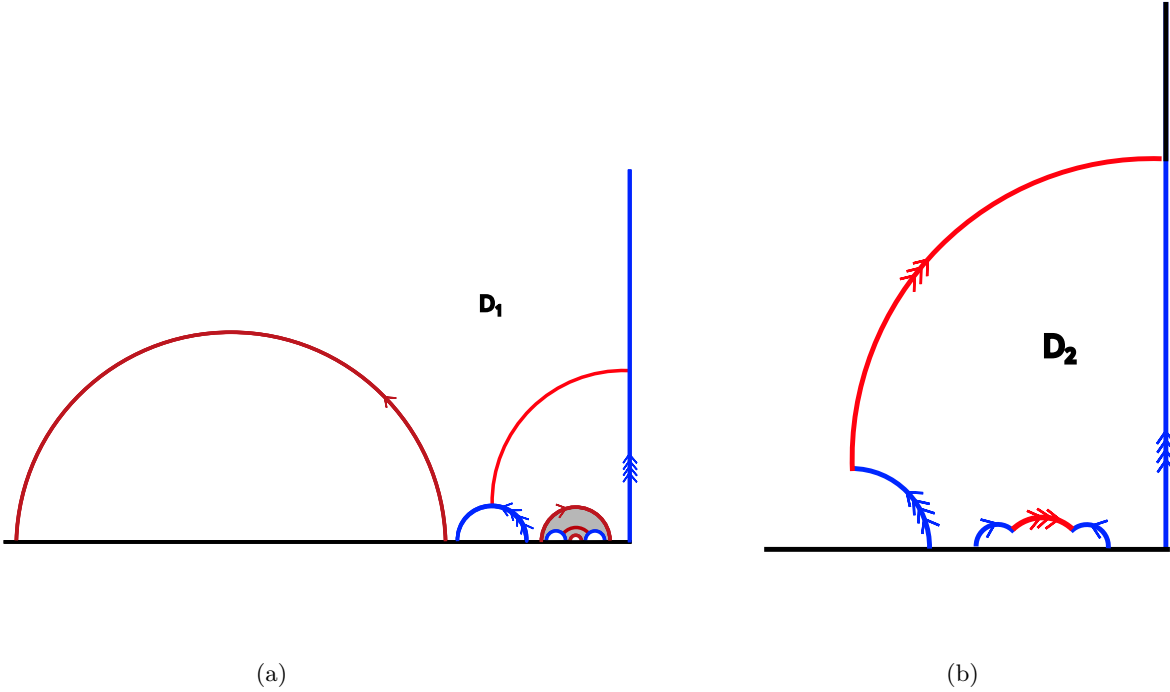


FIG. 6. **(a)** As in Figure 5(b), but showing also a geodesic arc (in red) that cuts D_1 in two symmetric halves, and the image of this arc in the shaded image of D_1 . **(b)** A new fundamental domain D_2 , combining half of D_1 and half of the shaded image of D_1 . The upper triple-arc boundary is mapped to the lower triple-arc boundary by \hat{A} . The left single-arc boundary is mapped to the right single-arc boundary by $\hat{A}\hat{B}\hat{A}^{-1}$.

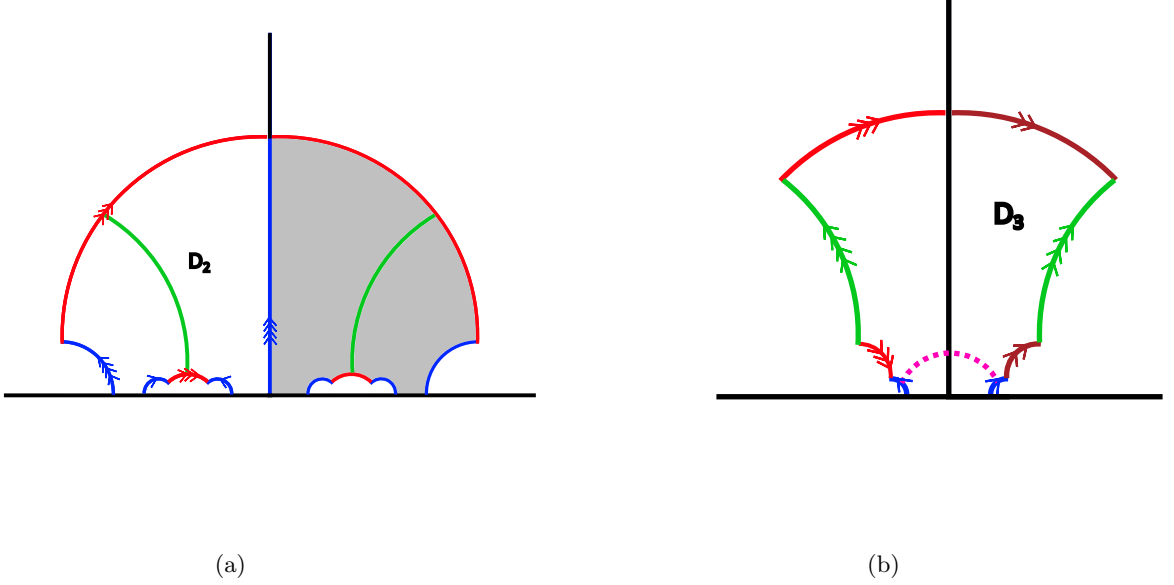


FIG. 7. **(a)** D_2 together with its image under \hat{B} , shown shaded. Also shown is a geodesic arc (in green) that cuts D_2 in two symmetric halves, and the image of this arc in the shaded image of D_2 . **(b)** A new fundamental domain D_3 , combining half of D_2 and half of the shaded image of D_2 . The left quadruple-arrowed boundary is mapped to the right quadruple-arrowed boundary by \hat{B} . The left single-arrowed boundary is mapped to the right single-arrowed boundary by $\hat{B}\hat{A}\hat{B}^{-1}\hat{A}^{-1}$, whose fixed points are $w = \pm 1$. The dashed curve is the geodesic circle joining $w = \pm 1$ and forming the horizon.

Appendix C: Topology

In this appendix we show that the quotient surface of the Poincaré disc is a punctured torus, and its fundamental group is the free group generated by $A/\{\pm 1\}$ and $B/\{\pm 1\}$, where A and B are given in (A6).

We start by representing the punctured torus as shown in Figure 8(a), as a punctured rectangle with the opposing sides pairwise identified as shown. We then perform a sequence of cut-and-paste deformations as shown in Figures 8(b)–10(a). The fundamental domain in Figure 10(a) is topologically identical to that in Figure 4(b), and the identifications by A and B in Figure 4(b) correspond to the pair of identifications across the boundaries of the fundamental domain in Figure 8(a). A perspective picture of the fundamental domain of Figure 7(b) glued across the identifications is shown in Figure 10(b).

As the fundamental group of the punctured torus is the free group generated by the two identifications shown in Figure 8(a) [33, Section 1.2][34], it follows that $A/\{\pm 1\}$ and $B/\{\pm 1\}$ provide a pair of free generators for the action of the fundamental group on the Poincaré disc.

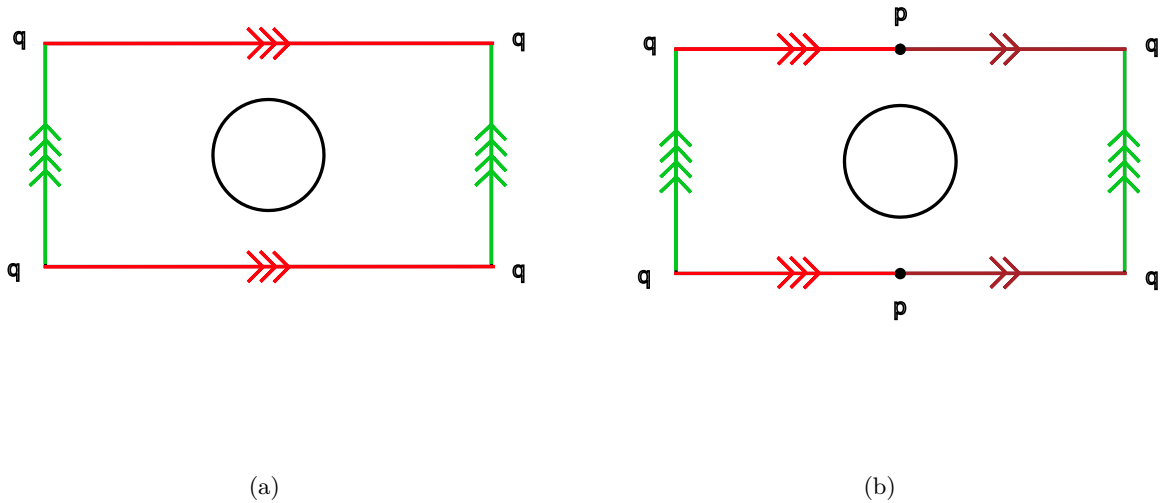


FIG. 8. (a) Fundamental domain of a punctured torus, realised as a rectangle with a hole in the middle. The arrows show the pairwise identifications of the sides. All the four corner points, labelled q , are identified. (b) A pair of identified points labelled p on the boundary are chosen. The double- and triple- arrowed boundary segments are identified.

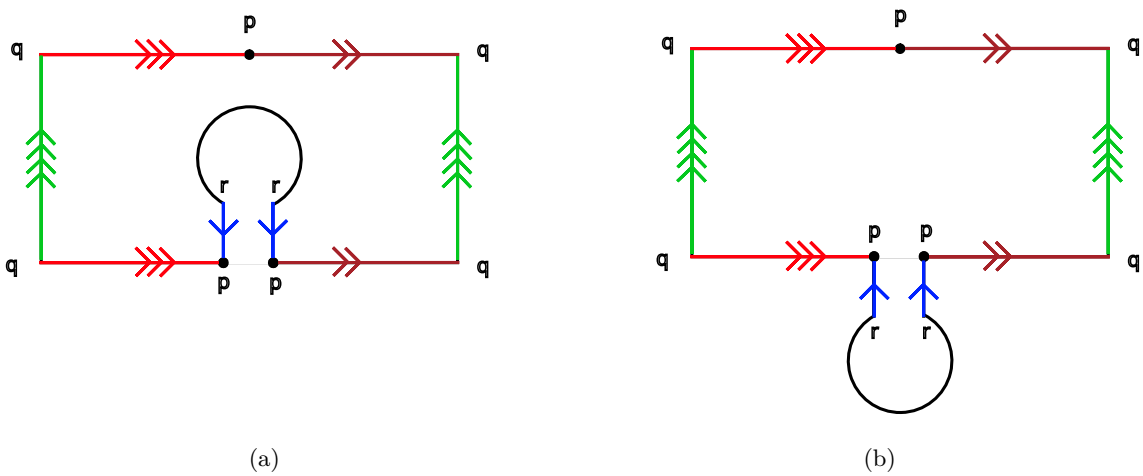


FIG. 9. (a) A cut is introduced from one of the points p to the puncture. (b) The surface is continuously deformed around the new cut.

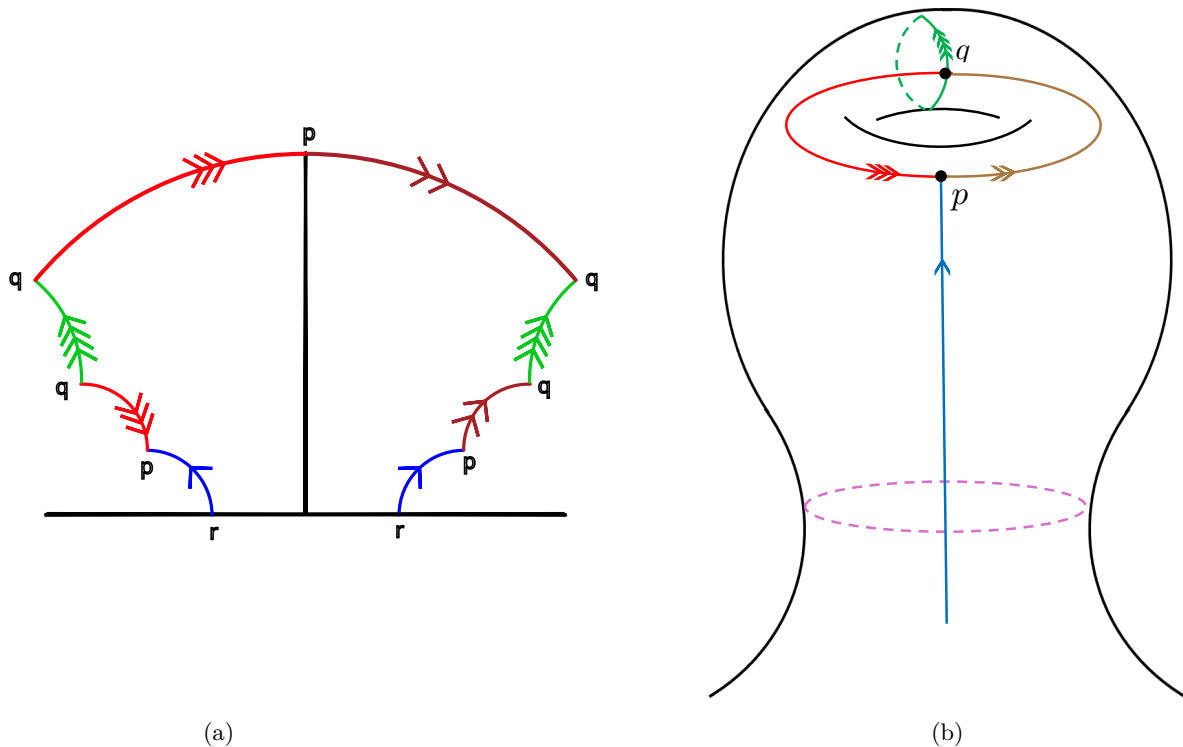


FIG. 10. (a) The straight boundary segments of Figure 9(b) are deformed to curved boundary segments that match those in the upper half-plane fundamental domain in Figure 7(b). (b) A perspective picture in which the fundamental domain of panel (a) has been embedded in \mathbb{R}^3 and glued across the identified boundaries. The top side of the surface in panel (a) has become the inner side in panel (b).

-
- [1] M. D. Kruskal, Maximal extension of Schwarzschild metric, *Phys. Rev.* **119**, 1743 (1960).
- [2] G. Szekeres, “Golden Oldie”: On the singularities of a Riemannian manifold, *Gen. Rel. Grav.* **24**, 2001 (2002), reprinted from *Publ. Math. Debrecen* **7** (1960), 285–301.
- [3] C. Fronsdal, Completion and embedding of the Schwarzschild solution, *Phys. Rev.* **116**, 778 (1959).
- [4] J. B. Hartle and S. W. Hawking, Path Integral Derivation of Black Hole Radiance, *Phys. Rev. D* **13**, 2188 (1976).
- [5] G. W. Gibbons and S. W. Hawking, Action Integrals and Partition Functions in Quantum Gravity, *Phys. Rev. D* **15**, 2752 (1977).
- [6] J. Louko and D. Marolf, Inextendible Schwarzschild black hole with a single exterior: How thermal is the Hawking radiation?, *Phys. Rev. D* **58**, 024007 (1998), arXiv:gr-qc/9802068.
- [7] J. Louko and D. Marolf, Single exterior black holes and the AdS/CFT conjecture, *Phys. Rev. D* **59**, 066002 (1999), arXiv:hep-th/9808081.
- [8] J. Louko, D. Marolf, and S. F. Ross, On geodesic propagators and black hole holography, *Phys. Rev. D* **62**, 044041 (2000), arXiv:hep-th/0002111.
- [9] D. E. Bruschi and J. Louko, Charged Unruh effect on geon spacetimes, in *12th Marcel Grossmann Meeting on General Relativity* (2010) pp. 2359–2361, arXiv:1003.1297 [gr-qc].
- [10] J. Louko, Geon black holes and quantum field theory, *J. Phys. Conf. Ser.* **222**, 012038 (2010), arXiv:1001.0124 [gr-qc].
- [11] A. R. H. Smith and R. B. Mann, Looking inside a black hole, *Class. Quantum Grav.* **31**, 082001 (2014).
- [12] R. D. Sorkin, Introduction to topological geons, in *Topological properties and global structure of space-time*, Proceedings of the NATO Advanced Study Institute on Topological Properties and Global Structure of Space-Time, Erice, Italy, May 12–22 1985, edited by P. G. Bergmann and V. De Sabbata (Plenum, New York, 1986) p. 249–70.
- [13] J. Louko, R. B. Mann, and D. Marolf, Geons with spin and charge, *Class. Quantum Grav.* **22**, 1451 (2005).
- [14] G. T. Kottanattu and J. Louko, Topological geon black holes in Einstein–Yang–Mills theory, *Commun. Math. Phys.* **303**, 127 (2011), arXiv:1001.4195 [gr-qc].
- [15] M. Bañados, C. Teitelboim, and J. Zanelli, Black hole in three-dimensional spacetime, *Phys. Rev. Lett.* **69**, 1849 (1992).
- [16] M. Bañados, M. Henneaux, C. Teitelboim, and J. Zanelli, Geometry of the (2+1) black hole, *Phys. Rev. D* **48**, 1506 (1993), [Erratum: *Phys. Rev. D* **88**, 069902 (2013)], arXiv:gr-qc/9302012.
- [17] S. Åminneborg, I. Bengtsson, D. Brill, S. Holst, and P. Peldán, Black holes and wormholes in 2 + 1 dimen-

- sions, *Class. Quantum Grav.* **15**, 627 (1998).
- [18] G. Lifschytz and M. Ortiz, Scalar field quantization on the (2+1)-dimensional black hole background, *Phys. Rev. D* **49**, 1929 (1994).
- [19] S. Carlip, The (2+1)-Dimensional black hole, *Class. Quantum Grav.* **12**, 2853 (1995), arXiv:gr-qc/9506079.
- [20] W. G. Unruh, Notes on black-hole evaporation, *Phys. Rev. D* **14**, 870 (1976).
- [21] B. S. DeWitt, Quantum gravity: The new synthesis, in *General Relativity: An Einstein Centenary Survey*, edited by S. W. Hawking and W. Israel (Cambridge University Press, Cambridge, England, 1979) pp. 680–745.
- [22] P. Langlois, Causal particle detectors and topology, *Annals Phys.* **321**, 2027 (2006), arXiv:gr-qc/0510049.
- [23] P. Langlois, *Imprints of spacetime topology in the Hawking-Unruh effect*, PhD thesis, University of Nottingham (2005), arXiv:gr-qc/0510127.
- [24] W. Junker and E. Schrohe, Adiabatic vacuum states on general space-time manifolds: Definition, construction, and physical properties, *Annales Henri Poincaré* **3**, 1113 (2002), arXiv:math-ph/0109010.
- [25] J. Louko and A. Satz, Transition rate of the Unruh-DeWitt detector in curved spacetime, *Class. Quantum Grav.* **25**, 055012 (2008), arXiv:0710.5671 [gr-qc].
- [26] A. Satz, Then again, how often does the Unruh-DeWitt detector click if we switch it carefully?, *Class. Quantum Grav.* **24**, 1719 (2007), arXiv:gr-qc/0611067.
- [27] L. Hodgkinson and J. Louko, Static, stationary and inertial Unruh-DeWitt detectors on the BTZ black hole, *Phys. Rev. D* **86**, 064031 (2012), arXiv:1206.2055 [gr-qc].
- [28] Smith, Alexander R. H., *Detectors, Reference Frames, and Time*, Ph.D. thesis, University of Waterloo (2017).
- [29] S. J. Avis, C. J. Isham, and D. Storey, Quantum Field Theory in anti-De Sitter Space-Time, *Phys. Rev. D* **18**, 3565 (1978).
- [30] M. R. Preciado-Rivas, M. Naeem, R. B. Mann, and J. Louko, More excitement across the horizon, *Phys. Rev. D* **110**, 025002 (2024), arXiv:2402.14908 [gr-qc].
- [31] S. Wang, M. R. Preciado-Rivas, M. Spadafora, and R. B. Mann, Singular excitement beyond the horizon of a rotating black hole, *Phys. Rev. D* **110**, 065013 (2024), arXiv:2407.01673 [gr-qc].
- [32] M. Spadafora, M. Naeem, M. R. Preciado-Rivas, R. B. Mann, and J. Louko (2024), in preparation.
- [33] A. Hatcher, *Algebraic Topology* (Cambridge University Press, 2002).
- [34] E. Dalvit, Punctured Torus, <https://www.youtube.com/watch?v=P5RLa3g-nwQ> (2010).